TABLE 2 Out-of-plane compressive properties (strain rate: 6.7×10^{-2} (s^{-1}))

	Liner	Corrugated medium
Young's modulus (MPa)	20.6 (17.4~22.6)	16.0 (13.1~18.8)

Average (min.-max.) for 10 samples

B. Experimental condition

Fig.2 shows the schematic of the experimental apparatus. The upper crosshead had a load cell with the maximum loading capacity of 10 kN. The front (outside) liner of the work sheet was attached to the lower crosshead. The heightwise flute of the work sheet was adjusted for being parallel to the view direction of CCD camera (Keyence digital microscope VHX-200, VH-Z35, picture element: 2,110,000 pixel). On the experiment apparatus, the upper crosshead moved downward with a feed velocity V of 0.05 $mm{\cdot}s^{-1}$.

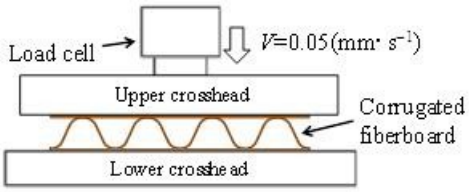

Fig.2 Schematic of flat crush test apparatus

Indentation displacement d of the upper crosshead was measured by a displacement meter of the servo actuator (Shinto Kogyo CYP-3-10, the position accuracy of +/–0.01mm.) until the inner flute was completely crushed between the inside liner (upper liner) and the outside liner (lower liner), while the reaction force F N (= specimen length 40 mm x width 10 mm x nominal pressure p MPa) was measured using the load cell. The CCD camera was used for recording video images as shown in Fig.3, in order to observe the deformation flow in the side view of the work sheet during the crosshead indentation. Sample numbers were 10.

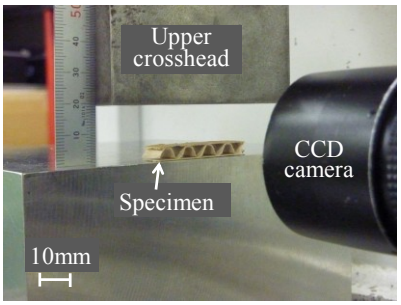

Fig.3 Observation unit and flat crush test apparatus

C. Crushing results of corrugated medium

Fig.4 shows the relationship between indentation depth of upper crosshead and nominal pressure for A-flute Cfbs. In this figure, the quasi-upper bound and the quasi-lower bound response were chosen from 10 samples and shown.

Fig.5 shows representative side views of rectangle-formed specimen during indentation of the upper crosshead for d/t= 0.0~0.4.

It was detected that there were three peaked points of load response at $d/t\approx$ 0.1, 0.2~0.3 and 0.4~0.5. As well-known, the first peak ($d/t\approx0.1$) appears to be a mode transition from the line joint structure, which is composed of CM and upper/lower liners, to the surface contact structure, which includes local-folding of glued zone.

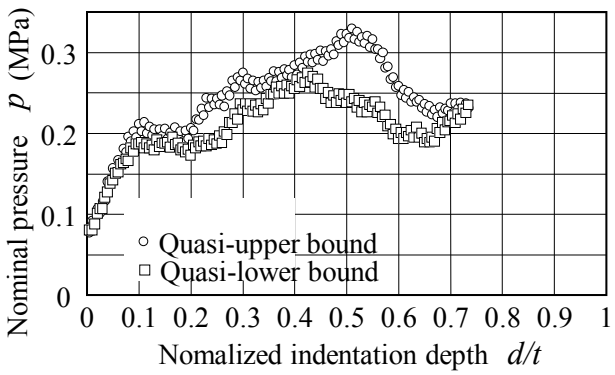

Fig.4 Load response of flat crush test of rectangle-formed specimen (t=5.1 (mm), V=0.05 ($mm{\cdot}s^{-1}$))

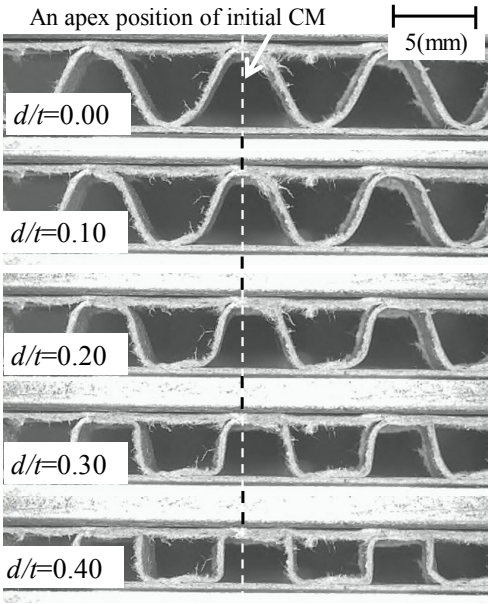

Fig.5 CCD camera photographs of side views of A-flute Cfb during flat crush test (t=5.1(mm), V=0.05 ($mm{\cdot}s^{-1}$))

The second-peaked position (d/t=0.2~0.3) appears to be a mode transition from the uniformly curved CM to the locally buckled CM. Namely, the semi-trapezoidal form of CM occurs at this position. This locally buckled form of CM is similar to the phenomena reported in Reference [5].

The third-peaked position (d/t=0.4~0.5) appears to be a mode transition from the semi-trapezoidal to the rectangle form of CM. These peaked positions (d/t) depend on the pre-stage processing, geometrical shape of CM and mechanical properties of raw-materials.

In this observation, it was found that the crushing form of CM was statistically asymmetric with respect to the lateral direction. Namely, the right side of CM wave tended to be easily folded. Dispersion of the secondary and third peaks seems to be caused by asymmetric folding between the right side and the left side of CM wave.

III. SIMULATION AND DISCUSSION

A. FEM Model

A finite element analysis code (MSC.MARC Ver. 2010. 1.0) with Updated-Lagrange procedure, large strain and non-linear contact function was used to simulate the upper crosshead indentation on an A-flute Cfb. The Cfb was considered as a deformable body, the lateral length of which

was four times of the wave length λ, as an orthotropic-elastic behavior with an orthotropic plastic behavior, while the upper/ lower crosshead were modeled as rigid contact bodies, as shown in Fig.6 (a).

The details of shape of CM were shown in Fig.6 (b), (c). The lower both ends (ends of lower liner) were rigidly fixed, while the upper liner was constrained by the coulomb friction model of the upper crosshead with the friction coefficient μ_{CH}=1.0.

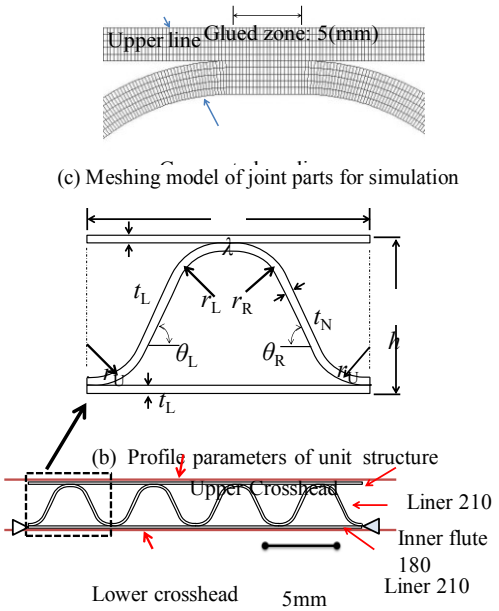

Fig.6 Simulation model of flat crush test of Cfb.

The friction coefficient between the liner and the CM was assumed to be 0.4 for the coulomb friction. Geometrical profile of A-flute Cfb was considered as two cases shown in TABLE 3. The profile parameters were measured from CCD camera photographs of Cfb at d/t=0, and simplified. Since the asymmetric model was based on measured values, the relation between the curvature radius of CM: $r_R > r_L$ was detected in this work.

TABLE 3 Profile parameters assumed in models

	Symmetric model	Asymmetric model
Height h (mm)	5.0	5.0
Wave length λ (mm)	9.0	9.06
Thickness of upper/ lower liners t_L (mm)	0.25	0.25
Thickness of inner flute t_N (mm)	0.25	0.25
Right radius r_R (mm)	1.7	1.8
Left radius r_L (mm)	1.7	1.7
Lower radius r_U (mm)	1.7	1.7
Right-inclined angle θ_R (°)	64.8	64.8
Left-inclined angle θ_L (°)	64.8	63.2

$$1/G_{MT} = (1+\nu_{MT})/E_M + (1+\nu_{TM})/E_T \quad (2)$$

$$1/G_{TC} = (1+\nu_{TC})/E_T + (1+\nu_{CT})/E_C \quad (3)$$

$$1/G_{CM} = (1+\nu_{CM})/E_C + (1+\nu_{MC})/E_M \quad (4)$$

In the case of orthotropic-elastic model, the moduli of transverse elasticity G_{MT}, G_{TC}, G_{CM} were calculated from Expressions (2), (3) and (4) that were shown by Campell [6]. For the Poisson's ratios ν_{MT}, ν_{TC}, ν_{CM}, the values measured by Baum et al. [7] were considered here.

TABLE 4 shows combination of elastic constants for FEM simulation. Over here, the suffixes are as follows: M: machine direction, C: cross machine direction, T: thickness direction. In the two-dimensional simulation model, the in-plane direction of liners and CM was assumed to be in MD.

TABLE 4 Combination of elastic constants for simulation

Raw-material	E_M (MPa)	E_T (MPa)	E_C (MPa)	ν_{MT}	ν_{TC}	ν_{CM}	G_{MT} (MPa)	G_{TC} (MPa)	G_{CM} (MPa)
Liner	5020	20	1884	0.2	0.01	0.2	20	20	1175
CM	4727	16	2046	0.2	0.01	0.2	16	16	1250

From the tensile testing of CM, the yield stresses σ_{YMD} =13.3 MPa, σ_{YCD}=5.0 MPa, σ_{Y45}= 10 MPa were estimated. The yield stress σ_{YTD} was assumed to be equal to σ_{YCD}, due to its difficulty of measurement [8]. The in-plane shear yield stress τ_Y=5.6 MPa was referred from [8]. Here, the suffixes denote the elongated direction of worksheet.

Hill's orthotropic yield criteria function (1948), which was implemented in MARC, was considered [9]. Using the specified expression of $\sigma_{ave} = (\sigma_{YMD} + 2\sigma_{Y45} + \sigma_{YCD})/4$= 9.6 MPa, the function parameters of MARC were determined as follow:

YRDIR(1)= $\sigma_{YMD}/\sigma_{ave}$ = 1.384,
YRDIR(2)= YRDIR(3)= $\sigma_{YTD}/\sigma_{ave}$ = 0.52,
YRSHR(1)= $\sqrt{3}\,\tau_Y/\sigma_{ave}$ = 1.009,
YRSHR(2)= YRSHR(3) = 1.0.

These values were applied to the corrugated medium.

The upper/lower liners were divided into height of 20% (five layers) and length of 10% thickness t_L with 7,240 elements for each, while the CM was divided into height of 20% and length of 10% thickness t_N with 10,400 elements. The four nodes 1st-order element type (plain strain) was used for simulating two-dimensional deformation.

Following four model conditions were considered for knowing the effect of asymmetric shape of CM and that of orthotropic properties.

1) Symmetric CM, orthotropic-elasto-plastic
2) Symmetric CM, MD based isotropic elasto-plastic
3) Asymmetric CM, orthotropic-elasto-plastic
4) Asymmetric CM, MD based isotropic elasto-plastic

Occurrence of asymmetric crushing of CM seems to be caused by combination of lateral freedom of liners and vivid-asymmetric shape of CM. Therefore, in the following, the boundary contact condition of upper linear was assumed to be constrained by the coulomb friction on the upper crosshead.

B. Load response

Fig.7 shows the relationship between the normalized indentation depth of upper crosshead d/t and the nominal crushing pressure p during the flat crush simulation.

In this work, the simulations of (a), (c) resulted in fault for d/t > 0.2 or 0.25.

When the MD based isotropic elasto-plastic models (b), (d) were simulated, the crushing pressure was raised up about 5MPa at d/t=0.2, while the actual crushing pressure was roughly 4% of (b), (d). Comparing Fig.7 with the MD based isotropic elasto-plastic models (b) and (d), it is found

that the stiffness in the thickness direction is a primary factor to determine the crushing reaction force.

From Fig.7, the following feature was detected: the first inflection point occurred at $d/t \approx 10\%$ when the orthotropic elasto-plasticity and the specified asymmetric shape of CM were considered. The saturation value of crushing pressure was close to the experimental result.

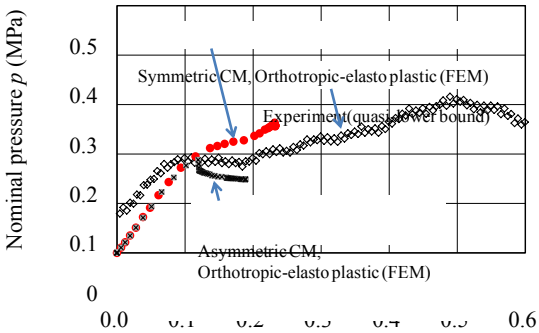

Fig.7 Relationship between indentation depth and crushing pressure on FEM simulation (in case of orthotropic-elasto-plastic model)

C. Crushing modes of corrugated medium

Fig.8 shows the crushing deformation of A-flute Cfb, which consists of a symmetric CM and upper/lower liners, with two material models for d/t=0.05, 0.15, 0.25, while Fig.9 shows that of asymmetric CM for two material models. Here, Fig.9 shows four cases of d/t=0.05, 0.10, 0.15 and 0.19, due to the simulation fault for d/t >0.2.

From these figures, the following features were detected:

1) The crushing mode of symmetric CM was kept in symmetric, while that of asymmetric CM moved in the lateral-right direction. Here, the asymmetrical condition had the relationship between the curvature radius of CM: $r_R > r_L$. This tendency matched to the experimental result.

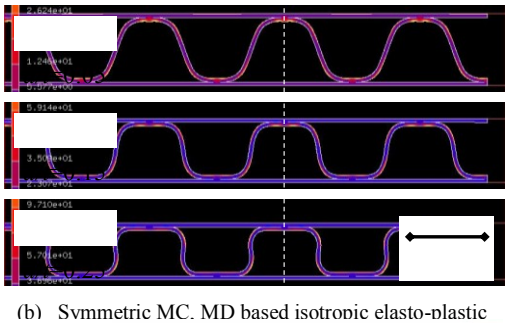

(b) Symmetric MC, MD based isotropic elasto-plastic

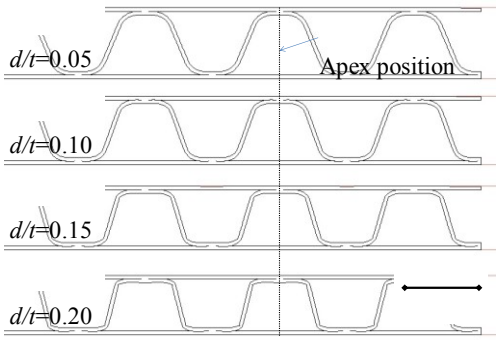

(a) Symmetric MC, orthotropic-elasto-plastic

Fig.8 Crushing in case of symmetric CM model

2) Comparing Fig.8 (b) with Fig.9 (b), the rectangle-formed wave (at d/t>0.15) of asymmetric CM had uneven pitch for the upper apex and the lower apex of the rectangle-formed wave. This tendency was similar to the experiment (Fig.5). 3) In the case of $r_R > r_L$ as shown in Fig.9 (a), a locally folded (buckling) position of the right side was a little far from the apex position of CM, compared to the left side folded position. 4) In the case of orthotropic-elasto-plastic model, locally folded points appeared to be sharply bent on the wave of CM. When a MD based isotropic elastic model was considered with the symmetric and asymmetric CM, the locally folded shapes were relatively round compared to the orthotropic-elasto-plastic model. Hence, the orthotropic property appears to accelerate the occurrence of buckling in a middle position.

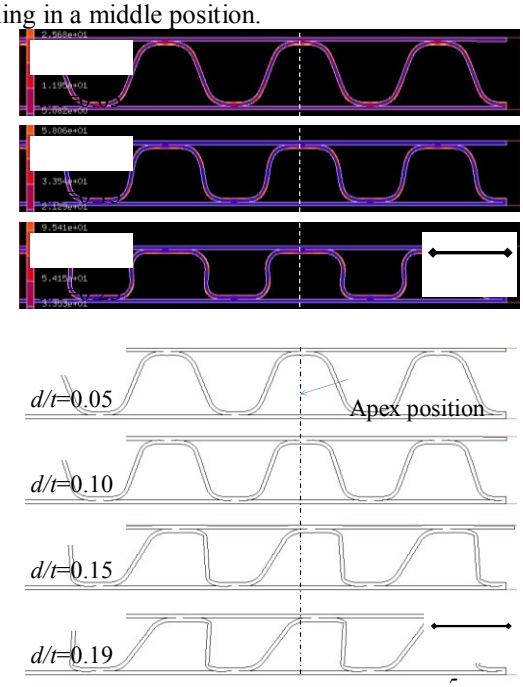

(a) Asymmetric MC, orthotropic-elastic

Fig.9 Crushing in case of asymmetric CM model

Compared the simulation results with the experiment (Fig.5), the locally folded shapes were fairly similar with each other, and the apex zones were almost in flat contact with the liners. Since this tendency seems to be caused by the in-plane sheared de-lamination of CM, such a de-lamination model of raw-materials (liners and CM) is necessary for further discussion. And also, the anisotropic plasticity of raw-materials seems to be another factor to characterize the crushing deformation of Cfb.

D. Discussion for asymmetric-lateral crushing

Reference [4] reported that the Z-like crushing of CM occurred in asymmetric for the setup position of a cutting blade from an apex position of CM, when the cutting blade (a symmetric wedge) was vertically indented to a heightwise C-flute Cfb. In this [4], a flat crush testing was discussed with respect to the right/left side inclined angles of CM wave. Since the inclined angles were globally defined (measured as the average angle of a triangle) from the combination of an upper apex position and a lower apex (root) position of CM wave, the current condition of A-flute Cfb must be compared with respect to the right/left side inclined angles. From TABLE 3, the equivalent wave length of asymmetric form was longer than that of the original form (symmetric wave). As the result, it is found that the

current asymmetric condition of A-flute Cfb has the same tendency as that of C-flute Cfb [4].

Since the asymmetric form of CM seems to statistically affect the occurrences of the Z-like crushing, which generate string-like paper dust, an advanced FEM simulation is required furthermore for predicting the asymmetric deformation of Z-like crushing.

E. Discussion for stress distribution at folding state

Fig.10 shows the contour lines of equivalent stress distribution on the CM for symmetric/asymmetric CM wave in case of orthotropic-elasto-plastic model. Here, the indentation depth was chosen as d/t=0.1, owing that the CM was just going to be buckled at the right side.

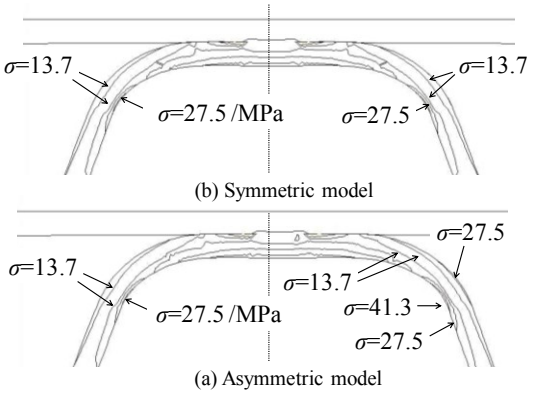

Fig.10 Equivalent stress distribution in case of orthotropic-elasto-plastic model (d/t=0.1)

In the case of asymmetric CM, the stress remarkably increased at the right side, where the radius of curvature was relatively larger than that of the left side. This seems to be caused by the difference of the half wave length (span of CM). A vivid-difference of geometrical shape causes the right side folding before the occurrence of left side folding.

IV. CONCLUSIONS

In order to investigate the deformation characteristics of an A-flute corrugated fiberboard (the constitutive basis weight: 210-180-210 g/m^2), a flat crush testing was experimentally and numerically applied to a rectangle-formed specimen. The followings were revealed through this study.

1) A vivid-asymmetric form of corrugated medium (CM) wave, of which the right side curvature radius r_R was larger than the left side r_L, tended to move in the right-lateral direction.
2) Orthotropic-elasto-plasticity of raw-materials and the vivid-asymmetric form of CM were primary factors to determine the crushing reaction force for the early stage (indentation depth of upper crosshead: $d/t \approx 0.1$).

ACKNOWLEDGMENT

This work was supported by the JSPS Grants-in-Aid for Scientific Research, Creative and Pioneering Research (C) of Grant Number 22560106.

REFERENCES

[1] Flat Crush Test of Corrugated Board (Flexible Beam Method), Test Method T 808 om-07, http://www.tappi.org/Bookstore/Standards--TIPs/Standards/Container-Testing/Flat-Crush-Test-of-Corrugated-Board-Flexible-Beam-Method-Test-Method-T-808-om-07.aspx, (accessed at 2nd of November, 2011)

[2] Japan Industrial Standard (JIS)-Z0403-1 (ISO 3035: 1982), Corrugated fibreboard – Part 1 : Determination of flat crush resistance, http:// www. jisc.go.jp/app/pager?id=45478 (accessed at 2nd of November, 2011)

[3] BusinessDictionaly.com, "flat crush test", http://www. Business dictionary.com/definition/flat-crush-test.html, (accessed at 14th of September, 2011)

[4] S. Nagasawa, M. Fujikura, Y. Fukuzawa, T. Kajizuka, "Deformation behavior of corrugated medium during wedge indentation into heightwise-corrugated paperboard", *Journal of Packaging Science and Technology JAPAN*, **20**-4, (2011) 283-292.

[5] B. K. Thakkar; L. G. J. Gooren; R. H. J. Peerlings; M. G. D. Geers, "Experimental and numerical investigation of creasing in corrugated paperboard", *Philosophical Magazine*, **88**-28, (2008) 3299-3310.

[6] J. Cambell, "The in-plane elastic constants of paper", *Applied Science* **12**-13, (1961) 356-357.

[7] G. Baum, D. Brennan, C. Habeger, "Orthotropic elastic constants of paper", Tappi Journal, **64**-86, (1981) 97-101.

[8] L.G.J. Gooren, Creasing behaviour of corrugated board, Master's thesis MT06.06, Technische Universiteit Eindhoven, February, (2006) 13-14.

[9] Hill, R. The mathematical theory of plasticity, Oxford University Press, (1950), London.